# Stub-Loaded Patch Antenna for Development of High Sensitivity Crack Monitoring Sensor

Nan-Wei Chen, *Member, IEEE*, Chih-Ying Chen, and Ren-Rong Guo

***Abstract*—This article proposes the use of a wireless sensor developed with a microstrip patch antenna in conjunction with an open-circuited stub for remote, real-time monitoring of crack width expansion. Technically, the open-circuited stub is exploited as a sensing structure with excellent sensitivity, and the crack growth is able to be mechanically mapped to the stub length extension via an incorporation of a mirrored stub structure placed right on top of the open-circuited stub. Thanks to a very strong relationship between the stub input admittance and its electrical length, the operating frequency of the patch is able to be significantly downshifted as the stub is mechanically lengthened (i.e., the crack grows). With the proposed wireless sensing scheme, the crack width expansion can be determined by identifying the dominant frequency component of the sensing signal received at remote data stations in a real-time manner. The sensor operating at 4 GHz was developed for experimental verification and as a demonstration of effectiveness. The experimental results show that the wireless sensor is able to identify the crack expansion of up to 2 mm with a resonant frequency downshift of 110 MHz. Furthermore, the maximum expansion and the finest increment can be simply specified with the sensor operating frequency regime. Moreover, a stable wireless link can be sustained as the patch radiation patterns remain unaffected while crack grows, and the sensor can be reused since the proposed monitoring does not result in any structure destruction or deformation.**

***Index Terms*—Crack, microstrip, patch, sensor, stub, wireless.**

## I. Introduction

NUMEROUS crack-growth monitoring technologies have been proposed and experimentally demonstrated, including piezoelectric transducers [1], [2], [3], fiber-optic sensors [4], [5], and antenna-based wireless sensors [6], [7], [8], [9], [10], [11], [12], [13], [14], [15], [16], [17], [18]. The wired sensing technologies [1], [2], [3], [4], [5] often call for lengthy cable or fiber connections and are costly in terms of system cost, installation, and maintenance. By contrast, the wireless sensors could be separately installed to monitor present cracks or the potential crack spots without physical connections between the sensors and data base stations, lending much greater flexibility in sensor network deployment. Technically, the wireless sensors fall into two categories, namely, passive [11], [12], [13], [14], [15], [16], [17], [18] and self-powered sensors [6], in accordance with operation power. Specifically, the self-powered (active) sensors use batteries or solar panels for sensing signal generation, while the power-up of passive sensors is realized with free-space feeding schemes, eliminating the need for periodical battery replacement and weather-related power shortages but leading to shorter sensor-to-station coverage. In theory, the passive crack sensors rely on the inducting coupling [11], [12] between two adjacent inductors or radio frequency identification (RFID) backscattering technique [13], [14], [15], [16], [17], [18] for crack monitoring. The sensing perimeter with the inductive coupling scheme is often limited to a few inches. To alleviate the limitation, RFID-based techniques, including the frequency doubling scheme [15], frequency and spatial division [16], and RFID chip incorporation [17], [18], have been proposed to uplift the sensing distance. However, the extended distance is still around a few meters, with a specified alignment between the sensor and the high-gain reader, and the sensing frequency regime is also restricted to the licensed RFID frequency bands, hindering its applications to small crack sensing. As for the sensing scheme, the frequency deviations of the received signals due to sensor structure deformation or destruction were adopted [7], [8], [9], [10], [11], [12], [13], [14], [15], [16], [17], [18]. For instance, the deviations due to a fracture on the ground of a patch antenna was presented in [8], and [15] reported the frequency offsets owing to the patch rupture. Unfortunately, the reported frequency offset due to small crack growth appears to be relatively small (a few MHz), which might potentially lead to challenging crack-width identification. Furthermore, the structural destruction or deformation could deteriorate the antenna radiation patterns and hinder sensor reuse. Specifically, the deteriorated patterns could lead to a failed wireless link with the high-gain RFID reader.

In order to tackle the aforementioned issues and further sensor deployment freedom, a sensing scheme requiring no destruction or deformation of the sensor structure is proposed. As depicted in Fig. 1, the wireless sensor mainly comprises a planar patch antenna and a mechanically extendable transmission line stub. The proposed scheme exploits the fact that resonant frequency of a microwave resonator could be perturbed by an external load [19]. Here, the microstrip-fed patch antenna [20] is adopted as the resonator, and a shunt microstrip open-circuited stub to the feed line is proposed as the external load structure to effectively vary patch resonant frequency. The proposed stub can be mechanically tailored to the crack expansion in such a manner

Manuscript received 6 December 2023; revised 4 February 2024; accepted 21 April 2024. Date of publication 29 April 2024; date of current version 22 May 2024. Recommended by Lead Guest Editor Pai-Yen Chen and Guest Editor Chung-Tse Michael Wu. *(Corresponding author: Nan-Wei Chen.)*

The authors are with the Department of Electrical Engineering, Yuan Ze University, Taoyuan 32003, Taiwan (e-mail: nwchen@saturn.yzu.edu.tw; s1104815@mail.yzu.edu.tw; s1108603@mail.yzu.edu.tw).

Digital Object Identifier 10.1109/JSAS.2024.3394393

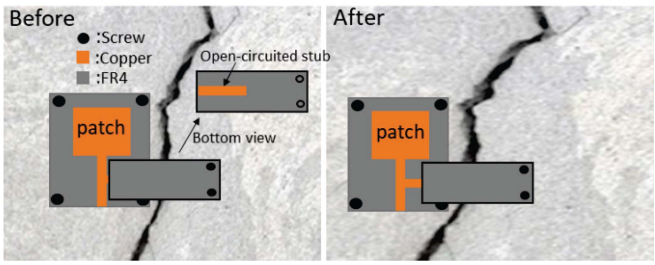


Fig. 1. Configurations of the patch antenna loaded with a mechanically extendable stub for concrete crack monitoring: (a) prior to the crack expansion and (b) after the crack expansion.

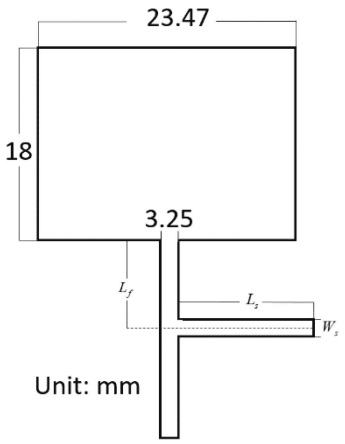


Fig. 2. Configuration and dimensions of the proposed wireless sensor.

that the stub lengthens while the crack grows. In theory, the open-circuited stub is essentially an impedance tuning element for input reflection suppression of the patch at a specified band of frequencies. It is know that the stub input admittance variation is a strong function of its length deviation, while the stub electrical length is in the vicinity of a quarter wavelength [19], [21]. Hence, with an external load of this kind, a large resonant frequency offset can be observed even with a small crack width increment. The maximum detectable crack growth and smallest increment are simply associated with the sensing frequency regime. That is, the patch with a lower resonant frequency aims to monitor large crack growth along with large, measureable increments.

The rest of this article is organized as follows. The proposed wireless sensing scheme for crack monitoring is demonstrated via the sensor realized with a stub-incorporated patch antenna at 4 GHz. Section II demonstrates the frequency characteristics of the microstrip patch antenna connected with an open-circuited stub of various electrical lengths as external loads. The proposed mapping of the crack growth to the stub extension is then presented. Section III details development of the measurement platforms for experimental verification along with the demonstration of experimental results to highlight the sensing effectiveness. Finally, Section IV concludes this article.

## II. Sensor Configuration and Characterization

As shown in Fig. 2, the proposed wireless sensor features a relatively simple configuration comprising a microstrip-fed patch antenna and a shunt open-circuited stub on the FR4 substrate ($\varepsilon_r = 4.4$) with a thickness of 1.6 mm and a stub length that can be mechanically extended. The input-reflection characterizations of the patch antenna loaded with the stub of various lengths and length extensions are first presented in Section A. The received signal intensity with a receiving patch antenna 30 cm away from the sensors is also demonstrated therein. Note that Ansys HFSS, the commercial full-wave electromagnetic solver, is adopted for the characterizations. Section B details the proposed avenue for the mechanical extension of the stub.

TABLE I
Dimensions of Three Stub Configurations

| $L_s$ | $W_s$ | $L_f$ |
|---|---|---|
| 6.6 (0.2$\lambda_g$) | 2.6 | 6.68 |
| 7.28 (0.22$\lambda_g$) | 1.4 | 7.28 |
| 7.95 (0.24$\lambda_g$) | 0.7 | 7.63 |

Unit: mm $\lambda_g$: guided wavelength in microstrip at 4 GHz.

### A. Stub-Loaded Patch Antenna

Again, aiming for a wireless sensor with high sensitivity, the patch antenna featuring a narrow operation band with a dominant operating frequency component was adopted. An external load capable of significantly shifting the operation frequency of the patch with a small length increment is proposed as the sensing element for crack growth monitoring. Specifically, the microstrip open-circuited stub is exploited as the external load since (1) relates the stub input admittance, $Y_{\text{in}}^o$, to its length, denoted as $L_s$, as

$$Y_{\text{in}}^o = jY_0 \tan \beta L_s \tag{1}$$

where $Y_0$ is the microstrip characteristic admittance and $\beta = 2\pi/\lambda_g$ is the propagation constant of the quasi-TEM wave of a guided wavelength, $\lambda_g$, travelling along the line [19], [21]. Based on the Taylor expansion, it can be deduced that the variation of $Y_{\text{in}}^o$ is inversely proportionally to the square of the stub length increment, which makes the stub a very effective tuning structure for achieving a large offset on the patch resonant frequency with a small length variation. Note that the imaginary part of the antenna input admittance at the resonant frequency is zero at resonance. In addition, a faster rate of admittance change is observed when the stub length is in the vicinity of multiple odd quarter wavelengths. On the contrary, past approaches [7], [8], [9], [10], [11], [12], [13], [14], [15], [16], [17], [18], which mainly relied on the destruction or deformation of the antenna geometry, result in relatively small resonant frequency deviations.

Fig. 3 demonstrates the simulated results of input reflection coefficients, namely, $S_{11}$ of the patch antenna loaded with stubs of various lengths, which gradually lengthen to 2 mm. Specifically, three investigated configurations along with the detailed dimensions are listed in Table I.

As shown in Fig. 3, all stub-loaded patches have reflection nulls at around 4 GHz with no stub extensions, and an apparent downshift of the reflection nulls is observed for three configurations. Specifically, the stub with the longest length (7.95 mm) results in the largest frequency offset of 90 MHz (4.05 to 3.96 GHz), with a 1 mm length extension, as presented in Fig. 3(c). The corresponding electrical length of this stub at 4 GHz is 0.24$\lambda_g$. By contrast, the results

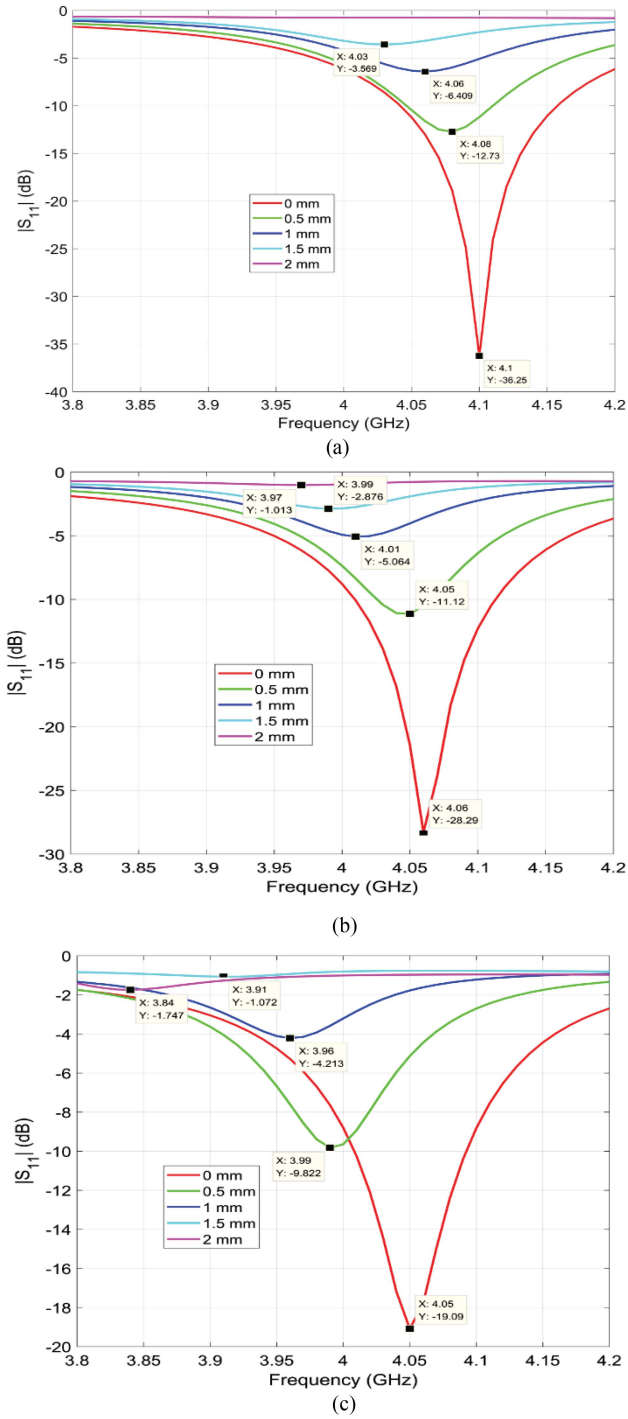


Fig. 3. Variations of the simulated input reflection coefficients of the stub-loaded patch at various stub length extensions while the stub is of the electrical length (a) $0.2\lambda_g$, (b) $0.22\lambda_g$, and (c) $0.24\lambda_g$.

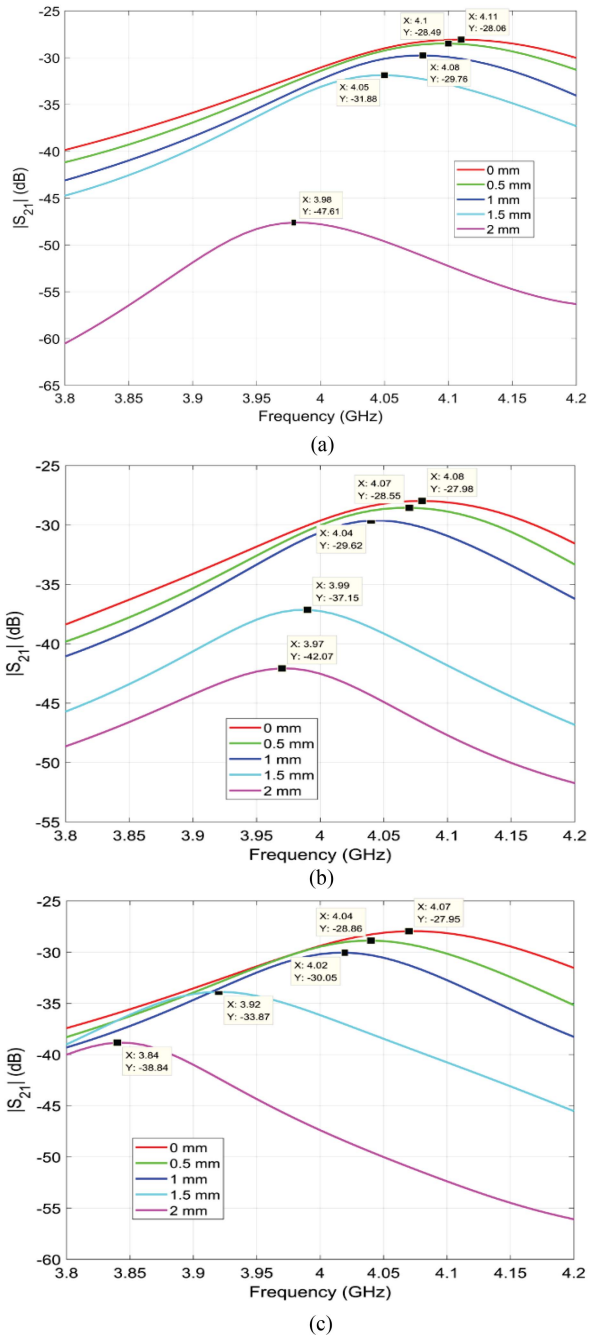


Fig. 4. Variations of the simulated transmission coefficients of the sensor at various stub length extensions while the stub is of the electrical length (a) $0.2\lambda_g$, (b) $0.22\lambda_g$, and (c) $0.24\lambda_g$.

presented in Fig. 3(a) and (b), 6.6 mm ($0.2\lambda_g$) and 7.28 mm ($0.22\lambda_g$), respectively, feature relatively small variations of the frequency nulls, and the frequency offsets are both 50 MHz with the same extension. Indeed, all stub configurations feature apparent reflection nulls relocations while stub lengthens, and the largest offset is 210 MHz for the $0.24\lambda_g$ stub with a 2 mm extension in length. Note that the marker annotation for the 2-mm extension case in Fig. 3(a) is not included as there is no identifiable null in the targeted frequency range (3.8–4.2 GHz).

To demonstrate the same operating frequency shift at the receiving end, Fig. 4 shows the simulated intensity of the received signal, viz. $|S_{21}|$, with a receiving patch antenna 30 cm away from the sensor, while the loaded stub of the three configurations has a length extension of up to 2 mm. Similarly, the $0.24\lambda_g$ stub '[see Fig. 4(c)] leads to a relatively large peak frequency offset of 230 MHz with a length extension up to 2 mm compared with

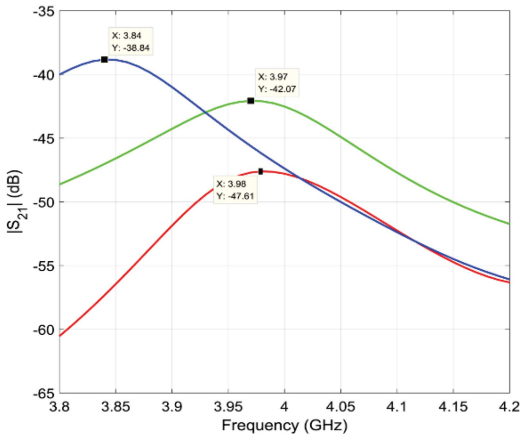


Fig. 5. Peak frequency location and intensity of the received signals for stubs of lengths $0.2\lambda_g$ (red), $0.22\lambda_g$ (green), and $0.24\lambda_g$ (blue).

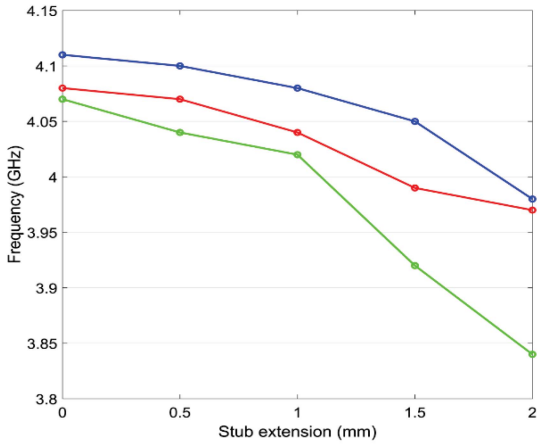


Fig. 6. Simulated downshift of the sensing signals at various stub length extension while the stub is of the electrical length $0.2\lambda_g$ (blue), $0.22\lambda_g$ (orange), and $0.24\lambda_g$ (green).

those with frequency offsets of 130 and 110 MHz shown in Fig. 4(a) and (b), respectively. Note that the receiving patch is designed with an operating frequency centered in the offset range corresponding to the reflection null offsets of the sensor with a specified stub length. Fig. 5 demonstrates the peak frequencies of the received signals for the three stub configurations at a length extension of 2 mm. Again, it is shown that the $0.24\lambda_g$ stub leads to the largest frequency downshift due to the fact that the admittance of the stub with a length in the near vicinity of a quarter of a wavelength has a faster rate of admittance change.

Specifically, Fig. 6 compares the simulated peak frequency downshifts of the above-investigated three stub configurations.

It is shown that the proposed sensing scheme is able to effectively identify the small crack increment as the apparent frequency deviations are observed.

### B. Tailoring of Crack Expansion to Stub Extension

As depicted in Fig. 7., the crack growth can be exactly mapped to the stub length extension via the following steps:

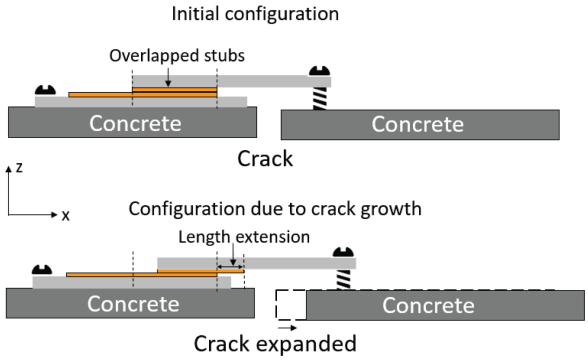


Fig. 7. Configurations of the patch antenna loaded with a mechanically extendable stub for concrete crack monitoring (a) prior to the crack expansion and (b) after the crack expansion.

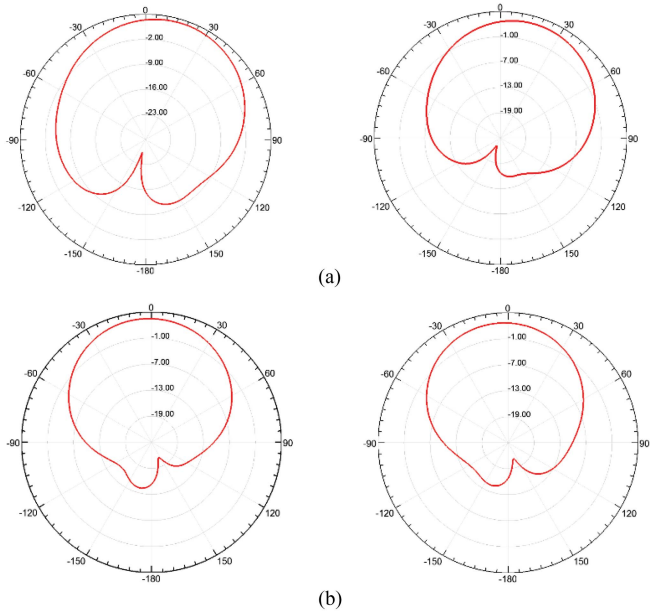


Fig. 8. Normalized copolarization radiation patterns of the wireless sensor with no extension (left column) and a 2 mm extension (right column) at (a) XZ plane and (b) YZ plane (all in dB).

1) duplicating the above-investigated open stub on the FR4 substrate;
2) flipping the duplicated version of the stub and placing it right on top of the open stub on the sensor;
3) anchoring the duplicated version to one end of the crack and attaching the stub-loaded patch to the other hand.

With this configuration, the crack growth results in a lengthened stub. Most importantly, dissimilar to the designs reported in [7], [8], [9], [10], [11], [12], [13], [14], [15], [16], [17], [18], the crack growth does not result in any structural damages or deformations, which makes sensor reuse possible. Moreover, as demonstrated in Fig. 8, the copolarization radiation patterns of the entire wireless sensor remain nearly unaffected with the proposed shape-preserving approach while the stub lengthens 2 mm, which is crucial to maintaining a stable and directional wireless link with the remote data stations.

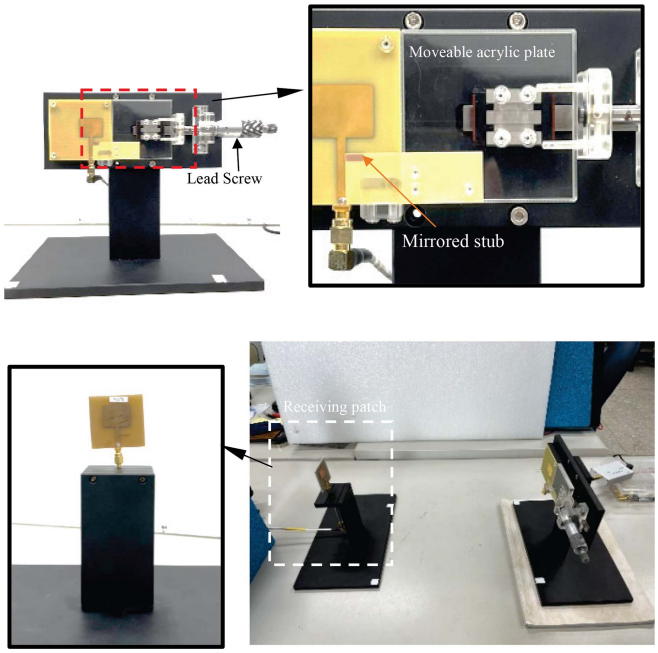


Fig. 9. Photos of the developed platform that was employed to verify and demonstrate the effectiveness of the proposed sensing scheme, as well as the measurement setup for the wireless transmissions.

## III. Sensor Development and System Verification

To demonstrate the effectiveness of the proposed sensing scheme for remote crack monitoring, an experimental platform that mimics the crack growth is built and shown in Fig. 9. On the sensing end, the duplicated stub is fixed to a moveable acrylic plate with plastic screws, and the plate can then be mechanically moved with a lead screw to mimic the crack expansion. In addition, the lead screw features a finest adjustment of 0.01 mm. The patch-based wireless sensor is fixed to a black wood stand with plastic screws to resemble its attachment to a concrete wall. Two experiments were conducted to demonstrate effectiveness, as discussed in the sections below.

### A. Effectiveness of the Sensing Scheme

The experiment calls for the use of a two-port vector network analyzer (VNA) to validate the above-observed frequency offsets of the input reflection and transmission coefficients due the stub extension. Specifically, the sensing signal is generated using the portable VNA, Anritsu MS2721A, and the signal is received with a receiving patch antenna on a black wood stand that is 30 cm away from the sensor and connected to the other port of the VNA. The sensor input reflections of the above-investigated sensor configurations with stub extensions up to 2 mm are respectively demonstrated in Fig. 10(a)–(c). As shown in Fig. 10(c), the $0.24\lambda_g$ stub experiences the largest downshift of 60 MHz, while the crack grows to 1.5 mm. By contrast, the 0.2 and $0.22\lambda_g$ stubs shown in Fig. 10(a) and (b), respectively, both have a 70 GHz frequency offset with a crack growth of 1.5 mm. The experimental results are in good agreement with the simulated ones presented above.

The corresponding measured transmission coefficients are presented in Fig. 11. As shown in Fig. 11(a), with a $0.2\lambda_g$ stub,

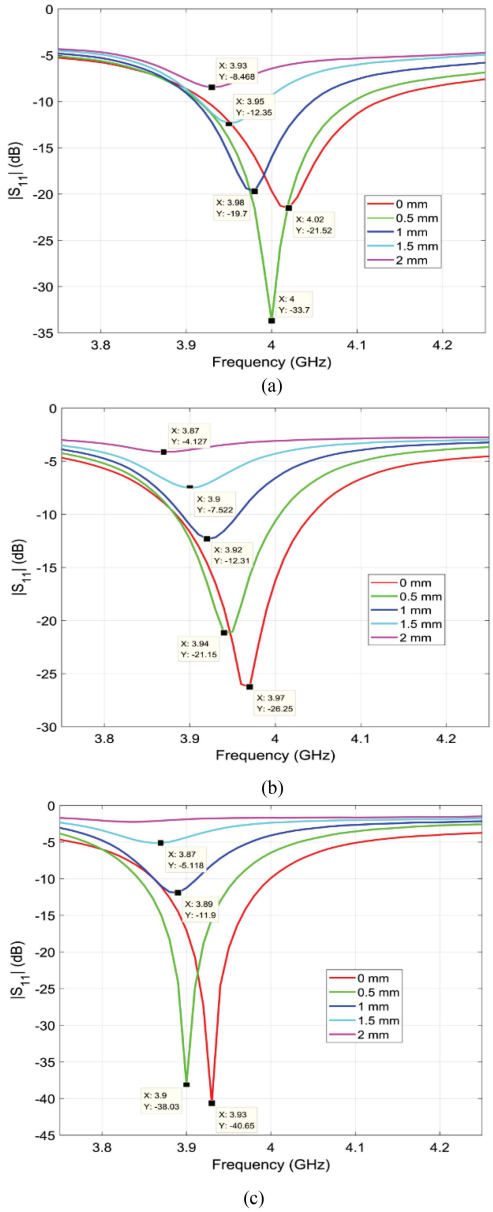


Fig. 10. Variations of the measured input reflection coefficients of the stub-loaded patch at various stub length extensions while the stub is of the electrical length (a) $0.2\lambda_g$, (b) $0.22\lambda_g$, and (c) $0.24\lambda_g$.

the deviations of location and intensity of the peak component of the received signal are not obvious until the crack growth is greater than 1 mm. Moreover, the frequency offset is 50 MHz for an expansion of 2 mm alongside a 2.65 dB intensity drop. By contrast, the 0.22 and $0.24\lambda_g$ stubs have relatively large variations in the location and intensity of the peak component of the received signal, as shown in Fig. 11(b) and (c), respectively. Specifically, the corresponding offsets are 100 and 110 MHz and the intensity variations are 7.59 and 9.68 dB, respectively.

### B. System Effectiveness

To demonstrate the proposed sensing effectiveness from a system perspective, the experiment setup resembling the practical crack monitoring is depicted in Fig. 12. Here, the sensing

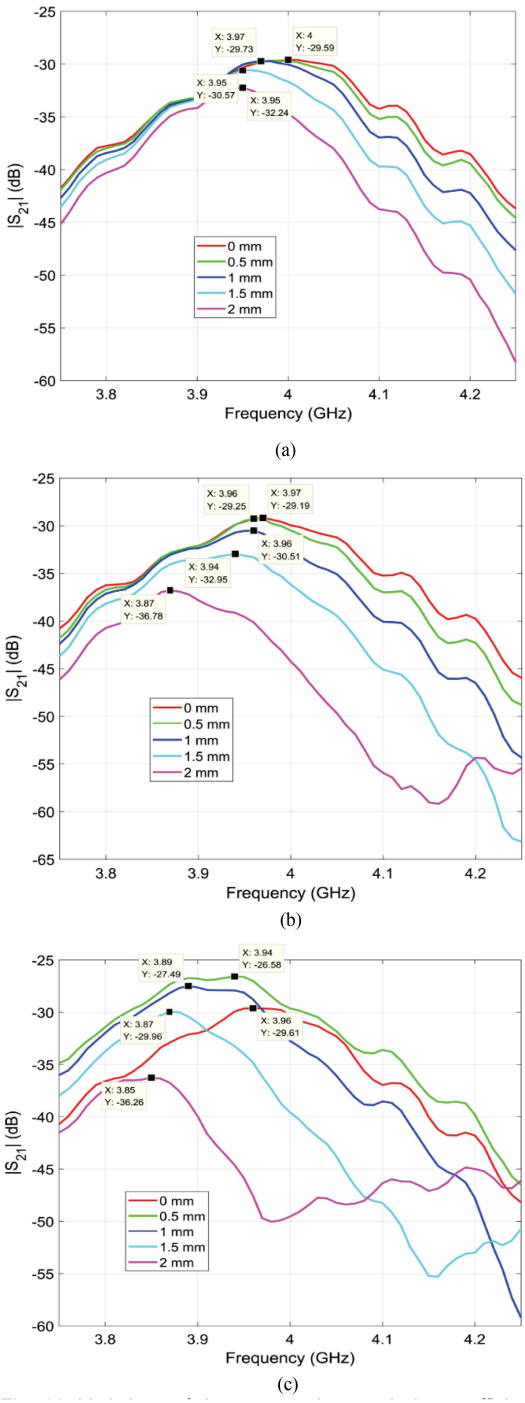


Fig. 11. Variations of the measured transmission coefficients at the receiving patch for the sensor with various stub length extensions while the stub is of the electrical length (a) $0.2\lambda_g$, (b) $0.22\lambda_g$, and (c) $0.24\lambda_g$.

signal is generated with a commercial noise source generator (3–6 GHz) that is able to be powered by a solar panel. Similarly, a receiving patch antenna with the operating frequency centered in the offset range is employed as the receiving antenna, and the received signal is then fed into a signal analyzer, the Keysight N9010A, interfaced with an Arduino Uno to identify the peak component frequency. Fig. 13 presents a sample spectrum of the received signal, and the exact peak frequency is determined with

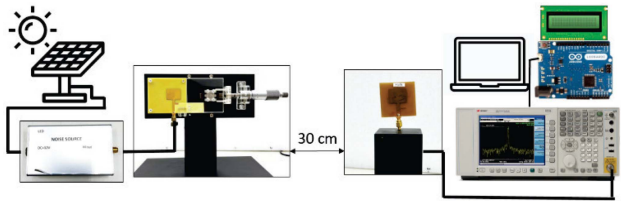


Fig. 12. Experimental setup for demonstration of the wireless crack monitoring system's effectiveness.

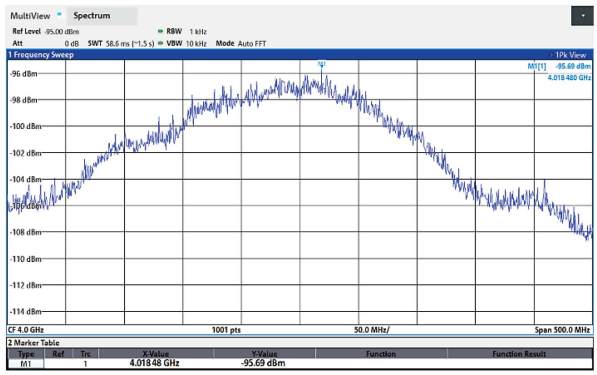


Fig. 13. Sample spectrum of the received sensing signal.

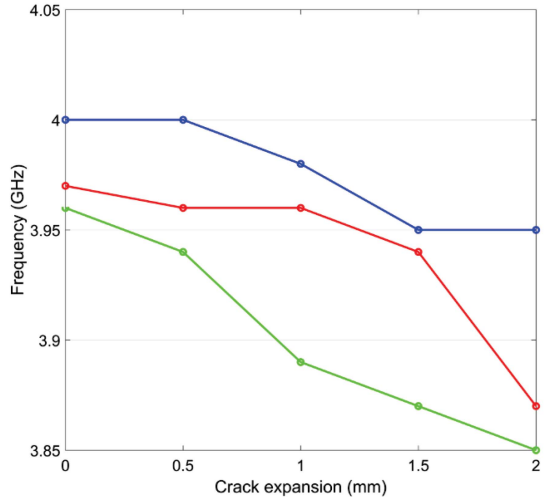


Fig. 14. Measured downshift of the sensing signals at various stub length extensions while the stub is of the electrical length $0.2\lambda_g$ (blue), $0.22\lambda_g$ (orange), and $0.24\lambda_g$ (green).

the average of the five identified values from the signal analyzer over a 1-minute time span. The determined peak frequency is finally shown on a liquid crystal display (LCD) connected with the Arduino Uno.

The measured peak frequency deviations and length extensions for the three stub configurations are demonstrated in Fig. 14, where very good agreement with the abovementioned experimental results is observed. It is shown that the $0.24\lambda_g$ experiences a relatively large frequency offset (50 GHz) with the crack growth between 0.5 and 1 mm. The $0.22\lambda_g$ stub has a 70 GHz offset and the crack grows from 1.5 to 2 mm. The minor discrepancy between the simulated relationships shown

in Fig. 6 and the measured ones might be attributed to that the practical guided wavelengths slightly deviate from the theoretically estimated ones. For instance, the practical wavelength is slightly smaller than the estimated value so the $0.24\lambda_g$ stub is marginally over a quarter wavelength while the growth is greater than 1 mm, and the $0.22\lambda_g$ stub is in the near vicinity but less than a quarter wavelength while the crack expansion is greater than 1.5 mm.

## IV. Conclusion

In conclusion, we demonstrate a 4 GHz wireless crack monitoring sensor with high sensitivity via incorporating the transmission-line stub structure as an effective admittance/impedance tuning element in the resonant antenna structure. Specifically, the microstrip open-stub-loaded patch antenna was exploited as a sensing device to monitor remote crack growth. Using mechanical tailoring, the crack growth was mapped to the shunt stub length extension, and the slightly lengthened stub was able to significantly offset the patch operating frequency with a small, submillimeter crack increment. Indeed, the experimental results demonstrate that a downshift of up to 110 MHz is attained with an increment of 2 mm alongside a 70 MHz offset for a growth of 0.5 mm. Moreover, the maximum detectable growth, along with the minimum increment, is simply related to the frequency regime. Furthermore, the proposed sensor calls for no structure deformation for crack sensing, and the radiation characteristics remain unaffected during the crack expansion. Future work will focus on the realization of the sensor network with the proposed sensor.

## References


[1] F. K. Chang and J. B. Ihn, "Detection and monitoring of hidden fatigue crack growth using a built-in piezoelectric sensor/actuator network: I. Diagnostics," *Smart Mater. Structures*, vol. 13, pp. 609–620, Jun. 2004.

[2] V. Giurgiutiu, *Structural Health Monitoring: With Piezoelectric Wafer Active Sensors*, Amsterdam, The Netherlands: Elsevier, 2007.

[3] H. Mei, M. F. Haider, R. Joseph, A. Migot, and V. Giurgiutiu, "Recent advances in piezoelectric wafer active sensors for structural health monitoring applications," *Sensors*, vol. 19, pp. 383–403, Jan. 2019.

[4] C. K. Y. Leung, N. Elvin, N. Olson, T. F. Morse, and Y.-F. He, "A novel distributed optical crack sensor for concrete structures," *Eng. Fracture Mechanics*, vol. 65, pp. 133–148, Jan. 2000.

[5] R. di Sante, "Fibre optic sensors for structural health monitoring of aircraft composite structures: Recent advances and applications," *Sensors*, vol. 15, pp. 18666–18713, Jul. 2015.

[6] G. Park, T. Rosing, M. D. Todd, C. R. Farrar, and W. Hodgkiss, "Energy harvesting for structural health monitoring sensor networks," *J. Infrastructure Syst.*, vol. 14, pp. 64–79, Mar. 2008.

[7] M. Liu, B. Li, and H. Li, "A crack monitoring method based on microstrip patch antenna," in *Proc. Annu. Rel. Maintainability Symp.*, 2015, pp. 1–5.

[8] M. A. Polochè Arango, H. F. Guarnizo Mendez, and I. E. Diaz Pardo, "Crack detection using an electromagnetic sensor-antenna for structures," in *Proc. Congreso Internacional de Innovación y Tendencias en Ingenieria*, 2019, pp. 1–6.

[9] S. Deshmukh, X. Xu, I. Mohammad, and H. Huang, "Antenna sensor skin for fatigue crack detection and monitoring," *Smart Structures Syst.*, vol. 8, pp. 93–105, 2011.

[10] I. Mohammad and H. Huang, "Monitoring fatigue crack growth and opening using antenna sensors," *Smart Mater. Structures*, vol. 19, pp. 1–8, May 2010.

[11] J. C. Butler, A. J. Vigliotti, F. W. Verdi, and S. M. Walsh, "Wireless, passive, resonant-circuit, inductively coupled, inductive strain sensor," *Sens. Actuators A, Phys.*, vol. 102, pp. 61–66, Dec. 2002.

[12] Y. Jia, K. Sun, F. J. Agosto, and M. T. Quiñones, "Design and characterization of a passive wireless strain sensor," *Meas. Sci. Technol.*, vol. 17, pp. 2869–2876, 2006.

[13] X. Xu and H. Huang, "Battery-less wireless interrogation of microstrip patch antenna for strain sensing," *Smart Mater. Structures*, vol. 21, Oct. 2012, Art. no. 125007.

[14] C. Occhiuzzi, C. Paggi, and G. Marrocco, "Passive RFID strain-sensor based on meander-line antennas," *IEEE Trans. Antennas Propag.*, vol. 59, no. 12, pp. 4836–4840, Dec. 2011.

[15] C. Cho, X. Yi, D. Li, Y. Wang, and M. M. Tentzeris, "Passive wireless frequency doubling antenna sensor for strain and crack sensing," *IEEE Sensors J.*, vol. 16, no. 14, pp. 5725–5733, Jul. 2016.

[16] X. Xu and H. Huang, "Multiplexing passive wireless antenna sensors for multi-site crack detection and monitoring," *Smart Mater. Structures*, vol. 21, Dec. 2011, Art. no. 015004.

[17] X. Yi, T. Wu, Y. Wang, R. T. Leon, M. M. Tentzeris, and G. Lantz, "Passive wireless smart-skin sensor using RFID-based folded patch antennas," *Int. J. Smart Nano Mater.*, vol. 2, pp. 22–38, Jan. 2011.

[18] X. Yi, C. Cho, J. Cooper, Y. Wang, M. M. Tentzeris, and R. T. Leon, "Passive wireless antenna sensor for strain and crack sensing—Electromagnetic modeling, simulation, and testing," *Smart Mater. Structures*, vol. 22, Aug. 2013, Art. no. 085009.

[19] D. M. Pozar, *Microwave Engineering*. Hoboken, NJ, USA: Wiley, 2017.

[20] C. A. Balanis, *Antenna Theory: Analysis and Design*. Hoboken, NJ, USA: Wiley, 2016.

[21] K. C. Gupta, R. Garg, and I. J. Bahl, *Microstrip Lines and Slotlines*. Norwood, MA, USA: Artech House, 1979.


**Nan-Wei Chen** (Member, IEEE) received the B.S. degree in atmospheric science and the M.S. degree in space science from the National Central University, Chungli, Taiwan, in 1993 and 1995, respectively, and the Ph.D. degree in electrical engineering from the University of Illinois at Urbana-Champaign, Champaign, IL, USA, in 2004.

From 1998 to 2004, he was a Research Assistant with the Center for Computational Electromagnetics, University of Illinois. In 2004, he joined the Department of Electrical Engineering, National Central University, Taiwan, as an Assistant Professor. In 2010, he joined the Department of Communications Engineering, Yuan Ze University, Taoyuan, Taiwan, as an Associate Professor, where he is currently working as a Full Professor with the Department of Electrical Engineering. His research interests include microwave/millimeter wave circuit and antenna designs, computational electromagnetics, and periodic structures.

Dr. Chen was the recipient of the Raj Mittra Outstanding Research Award at UIUC in 2004. He has been a Vice Chairman of the IEEE Antennas and Propagation Society Taipei chapter since 2018.

**Chih-Ying Chen** was born in Taichung, Taiwan on 12 September, 1998. He received the B.S. degree in electronic engineering from Ming Chuan University, Taipei, Taiwan, in 2021. He is currently working toward the master's degree in electrical engineering with Yuan Ze University, Taoyuan, Taiwan.

His research interests include wireless sensors and microwave wave circuit and antenna designs.

**Ren-Rong Guo** was born in Taipei, Taiwan on 20 August, 1969. He received the B.S. degree in electronic engineering and the M.S. in engineering from the Minghsin University of Science and Technology, Xinfeng, Taiwan, in 1991 and 2015, respectively. He is currently working toward the Ph.D. degree in electrical engineering with Yuan Ze University, Taoyuan, Taiwan.

His research interests include microwave/millimeter wave circuit and antenna designs.